

Cite this: DOI: 10.1039/xxxxxxxxxx

ESI: Creasing in evaporation-driven cavity collapse

Matt P. Milner^a, Lihua Jin^b, and Shelby B. Hutchens^{*a}

Received Date
Accepted Date

Electronic Supplementary Information

DOI: 10.1039/xxxxxxxxxx

www.rsc.org/journalname

1 Characterization of Sylgard 184 at Room Temperature and Hydrated at 60 °C

Constitutive model parameters for Sylgard 184 under heated (60 °C), hydrated conditions are compared to those at room temperature in Table S1. For all mixing ratios the shear modulus is higher in the heated and hydrated sample. Of the J_{lim} values determined, only the 10:1 mixing ratio showed a statistically significant variation with environment (single factor, ANOVA, $F_{ratio} > 1$). However, the variation was small, only decreasing by 11%.

2 Quantification of Crease Morphology

Crease data is gathered from a time series of optical images. Creases in cavity surfaces were digitally traced by hand via a series of line segments using a routine written in Matlab. Examples of digitized creases are shown for 10:1 and 25:1 mixing ratios in Figure S1. Continuous segments were counted as a single crease having a total length equal to the sum of the segment lengths. For cavities having large numbers of creases (e.g., 25:1 in Fig. S1), only half of the visible surface is characterized and the total cavity statistics is determined by extrapolating to the remaining surface area (multiplying by 4). For all other cavities, the creases characterized on the one visible half are doubled to obtain the full cavity 'total crease length' and 'number of creases' plotted in Figure 6.

3 Cavitation Event Frequency

While rarely a cavity will deform to the point of becoming optically invisible (i.e., completely closed), not all cavities deform by large amounts. Occasionally, the liquid droplet cavitates before onset of creasing or shortly thereafter. Table S2 quantifies the frequency of early cavitation among the compositions tested. Droplets in the 10:1 mixing ratio have a relatively higher probability of cavitation shortly after creasing, which may be due to the higher pressure attained as compared to the droplets in the other

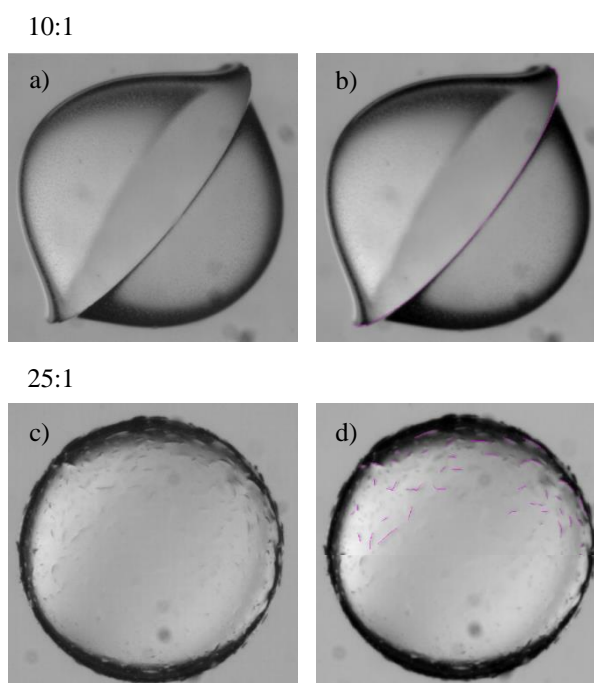


Fig. S1 Example crease images for 10:1 (a) and 25:1 (c) mixing ratios. Digitized creases are highlighted with magenta lines for the entire single crease (b) and, in the case of high crease number density, the upper half of the visible surface (d).

mixing ratios.¹

4 Crease Onset Interpolation

The critical strain for creasing can only be obtained via simulation using very small defect size as performed previously by Jin and Suo.² Using the results from their work relating crease onset, ϵ_c , to J_{lim} (Fig. S2, black squares), we interpolated to determine crease onset strains for experimentally measured J_{lim} values. These simulation data are fit via:

$$J_{lim} = A \exp(Bx^4) + \frac{C}{(x - 0.35)^2} + 3.1 \quad (S1)$$

^a Department of Mechanical Science and Engineering, University of Illinois Urbana-Champaign, Urbana, IL, USA.

^b Department of Mechanical and Aerospace Engineering, University of California Los Angeles, Los Angeles, CA, USA

*Tel: 1-217-300-0412 ; E-mail: hutchs@illinois.edu

Table S1 Shear moduli (μ) and strain hardening (J_{lim}) fit parameters from Eqn. 7 are reported for Sylgard 184 hydrated at 60 °C (H) and at room temperature (RT). The F_{ratio} from single factor ANOVA is given for the 10:1 and 12:1 mixing ratios.

Mixing Ratio	μ_H [MPa]	μ_{RT} [MPa]	J_{limH}	J_{limRT}	$F_{ratio,J_{lim}}$
10:1	0.55 ± 0.036	0.44 ± 0.042	6.2 ± 0.32	7.0 ± 0.62	1.25
12:1	0.39 ± 0.035	0.31 ± 0.022	18.1 ± 6.6	17.8 ± 6.7	0.001
17.5:1	0.20 ± 0.009	0.11 ± 0.019	NH	NH	N/A
25:1	0.073 ± 0.004	0.028 ± 0.004	NH	NH	N/A

Table S2 Number of droplets cavitating before creasing, shortly after creasing, or well after creasing for each observed mixing ratio. Droplets can take up to 48 hours to cavitate after creasing.

Mixing Ratio	Cavitation Before Creasing	Cavitation ≤ 4 hrs Post Crease	Cavitation > 4 hours Post Crease
10:1	3	4	2
12:1	1	0	5
17.5:1	0	0	8
25:1	1	2	4*

*One droplet completely closed.

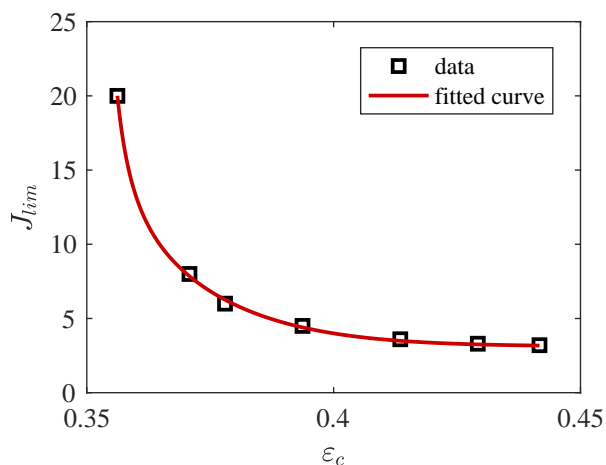


Fig. S2 Data (black squares) of predicted crease onset from Jin and Suo² fit to Equation S2.

The form of equation S1 was selected due to its ability to capture the limiting behaviors previously observed. That is, it predicts a neo-Hookean crease onset value as $J_{lim} \rightarrow \infty$ and predicts crease suppression as $J_{lim} \rightarrow 3.1$. The fit parameters, determined via least squares, are: $A = 415.5$, $B = -246.3$, $C = 3.469 \times 10^{-4}$.

5 Strain Hardening

A given strain hardening parameter, J_{lim} , corresponds to a specific limiting deformation state, depending on the type of loading. The stretch at which strain hardening occurs under equi-biaxial deformation is shown in Figure S3 and given by the expression:

$$J_{lim} = 2\lambda_{lim}^2 + \lambda_{lim}^{-4} - 3 \quad (S2)$$

6 ‘Microbubbles’ on Void Surface

Small ‘bubbles’ appear on the surface of the cavities shortly before creasing. Figure S4 provides typical close-up images of the ‘bubbles,’ thought to be un-crosslinked silicone polymer extracted

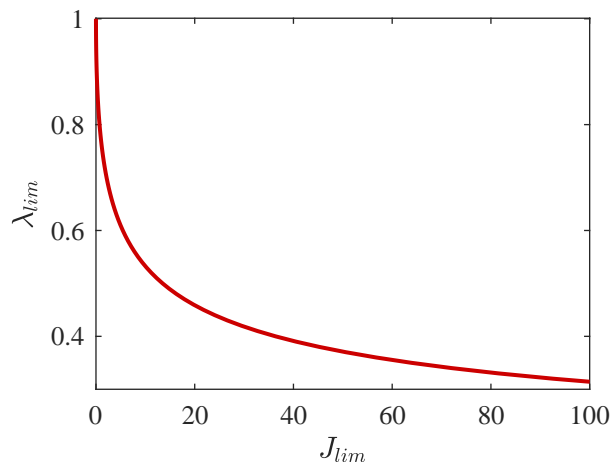


Fig. S3 Corresponding limiting stretch value, λ_{lim} for a given J_{lim} .

from the bulk polymer due to the high tensile loads in the water and large compressive deformations at the cavity surface.

7 Finite Element Simulation

A cavity of radius A within a cylinder of outer radius $B = 10A$ is used to approximate the deformation observed in liquid-filled cavities. The ratio $B/A = 10$ was selected because it approximates the experimental geometry. Figure S5 illustrates the full geometry, defect geometry, and typical mesh refinement used throughout the reported simulations. Element sizes varied from approximately $10^{-4}A$ near the defect to $0.5A$ at the outer, traction-free boundary. A mesh convergence study on a neo-Hookean material having two creases (Fig. S6a) demonstrates that near crease onset, error in the strain energy, $\Delta\Pi/(\mu A^2)$ is anticipated to be on the order of 1×10^{-5} . A stronger dependence on strain energy near crease onset is found for defect size (Fig. S6b). For ease of convergence, particularly in the case of the Gent material response, we use a defect size of $A/100$ throughout. We zero the strain energy by subtracting the small energy value at crease onset as described in section 3.3.1 in order to extract the energetic minimum as a function of crease number.

References

- 1 T. D. Wheeler and A. D. Stroock, *Nature*, 2008, **455**, 208–212.
- 2 L. Jin and Z. Suo, *Journal of the Mechanics and Physics of Solids*, 2015, **74**, 68–79.
- 3 W. Hong, X. Zhao and Z. Suo, *Applied Physics Letters*, 2009, **95**, 111901.

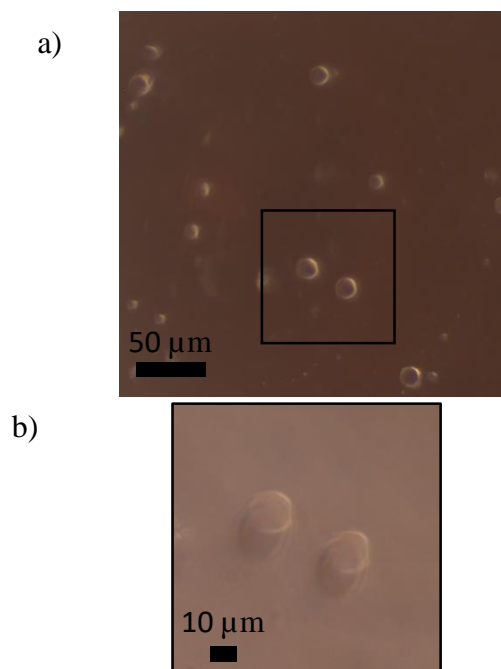


Fig. S4 Optical micrographs of the ‘microbubbles’ at the surface of a cavity within a 10:1 sample. a) The bubbles appear on about 5% of the surface and the magnified region b) A close up of the micron-sized bubbles.

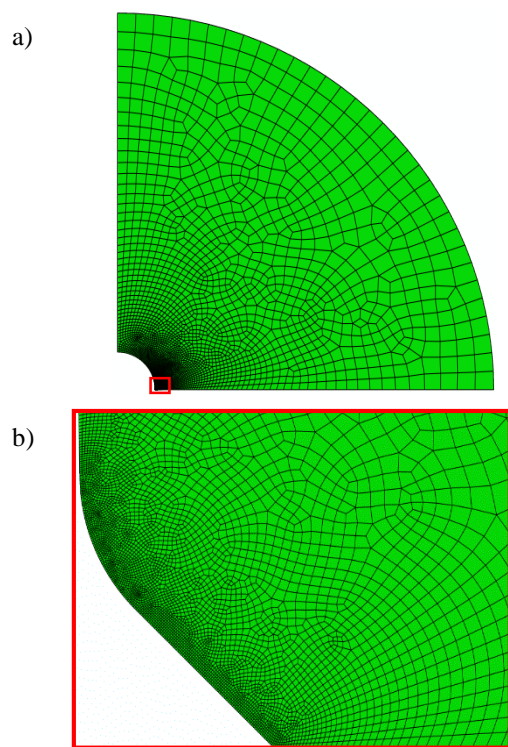


Fig. S5 Typical meshing used in FE simulation. a) The meshed cylindrical annulus showing refinement near the cavity surface. b) A close-up of the $A/100$ -sized defect, typical for all crease numbers simulated.

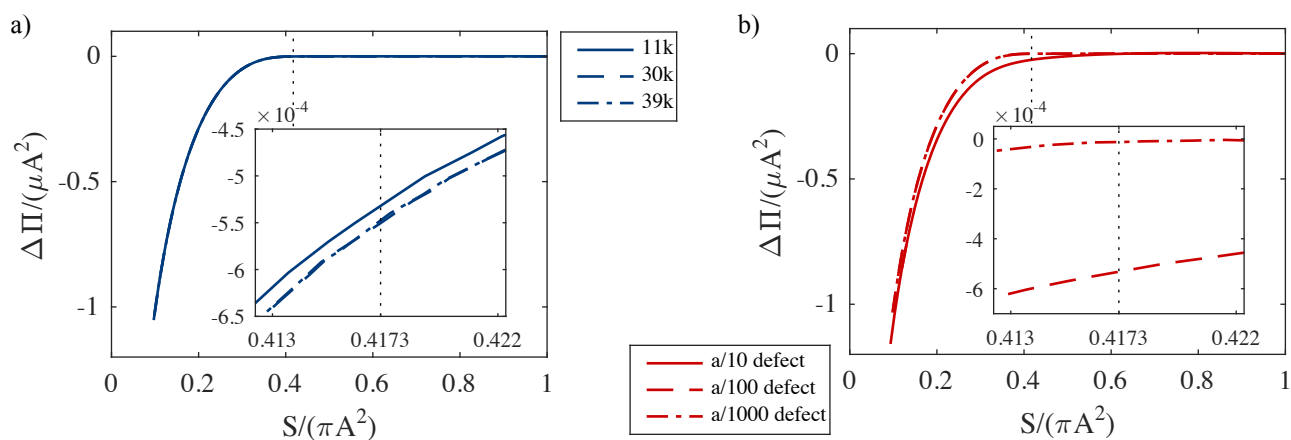


Fig. S6 Results from convergence studies of mesh refinement (a) and defect size (b) for a two crease geometry having a neo-Hookean material model. Crease onset in both figures is denoted with a vertical dotted line. a) Calculations were performed with 11k (solid), 30k (dashed), and 39k (dash-dot) elements corresponding to approximate element sizes of $A \times 10^{-4}$, $8A \times 10^{-5}$, and $7A \times 10^{-5}$, respectively around the defect. An $A/100$ size defect was used. b) Calculations using decreasing defect size show a strong dependence of strain energy near crease onset (as determined by previous simulation^{2,3}). Smaller defects approach a strain energy of zero at crease onset.